

# Fracture of Ni-Fe base metallic glasses

L. A. DAVIS

*Materials Research Center, Allied Chemical Corporation, Morristown, N.J., USA*

The fracture toughnesses of specimens of three transition metal base metallic glasses,  $\text{Ni}_{48}\text{Fe}_{29}\text{P}_{14}\text{B}_6\text{Al}_3$ ,  $\text{Ni}_{39}\text{Fe}_{38}\text{P}_{14}\text{B}_6\text{Al}_3$  and  $\text{Ni}_{49}\text{Fe}_{29}\text{P}_{14}\text{B}_6\text{Si}_2$  are reported. Each alloy was tested in a characteristic thickness, i.e., 25  $\mu\text{m}$  ( $\text{Ni}_{48}$ ),  $\sim 43 \mu\text{m}$  ( $\text{Ni}_{39}$ ) and  $\sim 72 \mu\text{m}$  ( $\text{Ni}_{49}$ ) and  $K_{\text{IC}}$  values of  $\sim 120$ , 62 and 30  $\text{kg mm}^{-3/2}$ , respectively, were observed. It is suggested that this variation is associated primarily with a transition from plane strain ( $K_{\text{IC}} \simeq 30 \text{ kg mm}^{-3/2}$ ) toward plane stress conditions as sample thickness is decreased. The fatigue crack propagation rate in the  $\text{Ni}_{39}$  alloy is also reported;  $da/dn$  (mm/cycle)  $\simeq 2 \times 10^{-8} \Delta K^{2.25}$ , where  $\Delta K$  has units of  $\text{kg mm}^{-3/2}$ . When the respective data are plotted in terms of  $(\Delta K/E)$ , where  $E$  is Young's modulus, the crack growth behaviour for the Ni-Fe glasses approximates that for crystalline ferrous alloys. A classical chevron pattern, macroscopically at  $90^\circ$  to the tensile axis, is observed when amorphous metallic alloy strips fracture under plane strain conditions. On a finer scale, the chevrons exhibit a sawtooth structure, and the sawtooth surfaces show a fine scale, equi-axed vein pattern. This indicates that local failure occurs by shear rupture.

## 1. Introduction

It has been observed that amorphous metallic alloys are distinguished by exceptional strength and distinctive deformation mechanics. For example, for alloys based on Pd strengths of the order of 150  $\text{kg mm}^{-2}$  are observed [1-3] while for those based on Ni and/or Fe tensile strengths of the order of 140 to 280  $\text{kg mm}^{-2}$  are observed [4, 5]. Deformation occurs in highly inhomogeneous shear bands [2, 6]. In compression many intense intersecting shear bands are active and little or no work hardening is observed [3, 7, 8], i.e. these materials appear to approximate elastic-perfectly plastic behaviour. On tensile loading deformation occurs in a singularly intense shear band and failure occurs coincident with local yielding [1-5]. The local shear strain to failure is of the order of 10 or more.

Characterization of the mechanical properties of metallic glasses based on the concepts of fracture mechanics was initiated recently when the mode III fracture toughness [9, 10] of a number of metallic glasses was determined in tear tests by Kimura and Masumoto [11]. To further develop the fracture mechanics characterization of these materials measurements of the mode I fracture toughness would be of interest. The purpose of the present paper,

therefore, is to report determinations of the fracture toughness of specimens which fail partially or fully in plane strain. Three closely related transition metal base Metglas®\* alloys,  $\text{Ni}_{48}\text{Fe}_{29}\text{P}_{14}\text{B}_6\text{Al}_3$ ,  $\text{Ni}_{39}\text{Fe}_{38}\text{P}_{14}\text{B}_6\text{Al}_3$  and  $\text{Ni}_{49}\text{Fe}_{29}\text{P}_{14}\text{B}_6\text{Si}_2$  are examined (subscripts refer to atomic percentages). The fatigue crack propagation rate in the  $\text{Ni}_{39}$  alloy is reported also.

## 2. Experimental procedure

### 2.1. Materials

The alloys studied were quenched to ribbons directly from the melt and adjudged to be amorphous by X-ray examination. The alloys in question were chosen because they were of similar composition and each happened to be available in a different thickness. The  $\text{Ni}_{48}$  alloy was prepared as narrow strips which were polished on their edges to produce strip 0.4 mm wide and  $\sim 0.026$  mm thick. The  $\text{Ni}_{39}$  alloy was produced as wider and thicker strips which, with polished edges, were  $\sim 1.7$  mm wide and  $\sim 0.042$  mm thick. The  $\text{Ni}_{49}$  alloy was  $\sim 0.76$  mm wide and  $\sim 0.072$  mm thick.

As produced, these alloys exhibit tensile strengths of 190  $\text{kg mm}^{-2}$  ( $\text{Ni}_{48}$ ), 214  $\text{kg mm}^{-2}$  ( $\text{Ni}_{39}$ ) and 240  $\text{kg mm}^{-2}$  ( $\text{Ni}_{49}$ ). For the latter two alloys this value was determined for specimens

\*Trade mark of the Allied Chemical Corporation, Morristown, N.J., USA.

with hand polished, reduced cross-section gauge lengths. Owing to the difficulty of handling such narrow strips the Ni<sub>48</sub> alloy was tested in the form of uniform cross section specimens which usually failed at the grips due to the elastic constraint which obtains there. Experience with the Ni<sub>39</sub> alloy suggests that the tensile strength may be 10 to 20% reduced in this configuration.

Hardness values (DPH), as determined with a Leitz Miniload hardness tester (Leitz, Wetzlar, Germany) (100 g load), were found to be 752 kg mm<sup>-2</sup> (Ni<sub>48</sub>), 752 kg mm<sup>-2</sup> (Ni<sub>39</sub>) and 792 kg mm<sup>-2</sup> (Ni<sub>49</sub>). (As the Ni<sub>48</sub> strips are of marginal thickness for valid DPH measurements, the value cited was determined on a thicker amorphous sample of the same alloy.) A sample of amorphous Pd<sub>77.5</sub>Cu<sub>6</sub>Si<sub>16.5</sub> also tested exhibited DPH  $\approx$  498 kg mm<sup>-2</sup>. On comparison with the yield strength of this alloy in compression [7] ( $\sigma_c \sim 160$  kg mm<sup>-2</sup>) one obtains a ratio DPH/ $\sigma_c \approx 3.1$ . We may infer then that the inherent yield stress (neglecting a possible normal stress dependence) for all three Ni-Fe alloys is of the order of 250 kg mm<sup>-2</sup>.

## 2.2. Toughness testing

Uniform cross-section Ni<sub>48</sub> strips were loaded under cyclic tension-tension conditions. Fatigue crack initiation generally occurred at one of the narrow edges of the strip so that the specimen then behaved as a single edge notch specimen. After failure, the specimens were examined in a scanning electron microscope to determine the crack size at the onset of rapid fracture. The fracture toughness could then be calculated using the programmed peak load in the load control fatigue programme.

The Ni<sub>39</sub> and Ni<sub>49</sub> strips were prepared for centre cracked panel fracture toughness tests. A hole of  $\sim 0.1$  mm diameter was placed in the centre of each specimen by electric discharge machining (EDM). A sharp crack was generated at the hole by cyclic loading of the specimen. For a few Ni<sub>39</sub> specimens cyclic crack growth was terminated and the specimens were pulled to failure at a constant stroke rate of 0.15 mm min<sup>-1</sup>. No further slow crack growth could be observed. The remaining specimens were allowed to fail during cyclic loading. In both cases the onset of fast fracture was clearly evident in the SEM.

## 2.3. Fatigue crack growth rate

For two Ni<sub>39</sub> strips the growth of fatigue cracks

was observed with a binocular microscope, incorporating a ruled grating. The cracks were sufficiently small so that they could be easily kept in the field of view at a magnification of  $\times 105$ . Plots of  $a$ , the crack half-length, versus  $n$ , the number of cycles were made and  $da/dn$  was determined graphically.

## 2.4. Mechanical testing equipment

All experiments were conducted using an electro-hydraulic servo-controlled mechanical testing machine (MTS Systems Corporation, Minneapolis, Minn., USA). Cyclic loading, with a sinusoidal wave form, was conducted in load control at a frequency on the order of 1 to 5 Hz, in which case the load signal was monitored by an amplitude measurement panel and displayed on an oscilloscope. For the constant stroke rate tests the load-time response was displayed on a strip chart recorder; the small size of the specimens precluded the use of a crack opening extensometer. Cyclic loading was conducted with a variable maximum stress ( $\sigma_{max}$ ) and a fixed minimum stress ( $\sigma_{min}$ ) of  $\sim 21$  kg mm<sup>-2</sup>, dictated by a desire to eliminate slack in the loading system.

The specimens were gripped in drum-clamp type grips as reported for a previous study [3]. These grips are arranged so that the specimen, located on the centre axis of the loading system, is unclamped where it exits each drum tangentially. Specimens were arranged with 2.54 cm between grip tangents.

All tests were conducted at room temperature ( $\sim 22^\circ\text{C}$ ) in the laboratory environment.

## 3. Results

### 3.1. Fracture topography

Fig. 1 shows the typical fracture topography for a centre cracked Ni<sub>39</sub>Fe<sub>38</sub>P<sub>14</sub>B<sub>6</sub>Al<sub>3</sub> specimen. Figure 1a and b are the two sections from either side of the EDM hole of a continuous fracture surface. The boundary of the EDM hole lies at the inside edge of each fractograph and the sharp demarcation between the slowly propagating fatigue crack and the onset of fast failure is clearly evident. The rapid fracture section exhibits a classic chevron pattern, typically observed in the fracture of steel plates [12]. Both the fatigue crack section and the rapid fracture section lie at  $90^\circ$  to the tensile axis on a macroscopic scale. Shear lips about  $2$  to  $4 \times 10^{-3}$  mm wide (a typical thickness for all three alloys) and at  $45^\circ$  to the tensile axis are

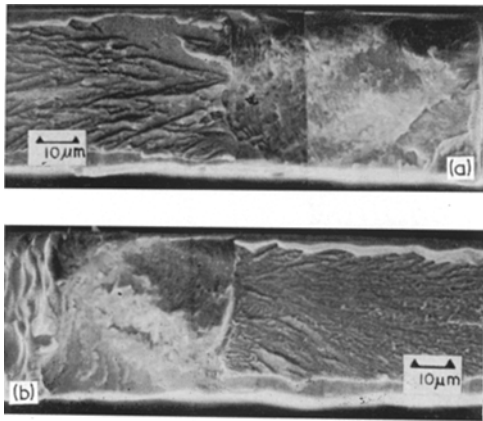


Figure 1 (a) and (b) Sections of a continuous fracture surface, located on either side of an EDM hole, of a  $\text{Ni}_{39}\text{Fe}_{38}\text{P}_{14}\text{B}_6\text{Al}_3$  metallic glass specimen examined in the scanning electron microscope. The edges of the hole lie at the middle of this partial montage. Adjacent to either side of the hole is the fatigue crack. A sharp boundary separates the fatigue crack and the rapid fracture surface, which lies at the outside extreme of each micrograph. A classical chevron pattern is evident on the brittle fracture surface. Shear lips lie on either side of the specimen. Except for the shear lips the fracture surface is macroscopically at  $90^\circ$  to the tensile axis. Outside the view of these micrographs the fracture surface assumed a slant configuration.

evident on either side of the rapid fracture surface. As the crack propagates, the plastic zone size increases so that the shear lips increase in width until the fracture surface undergoes transition from square (plane strain) to slant (plane stress). For the specimen shown the plane strain region covers  $\sim 1.1$  mm of the total 1.7 mm width. Typically, 50% or more of the fracture surface (beyond the fatigue crack) exhibits square fracture. We expect, therefore, that one may assume that catastrophic failure ensues immediately when the initial popin beyond the fatigue crack occurs. Hence the fracture tough-

ness  $K_C$  may be calculated using the half length of the fatigue crack and the peak load of the fatigue programme or stroke test.

Fig. 2 shows the fracture of a  $\text{Ni}_{49}$  specimen. In this case no transition to slant fracture is observed. Hence one may calculate  $K_C$  as just noted.

For the thin  $\text{Ni}_{48}$  specimens the fracture topography appears to depend on stress level. For relatively high nominal stress the transition from square to slant occurs over a distance which is small compared to the specimen width. For relatively low nominal stress there is a clearly defined, extended, intermediate region between the end of the fatigue crack and the beginning of a "normal" square fracture. Behaviour typical of high stress is shown in Fig. 3. The plane strain crack is observed to extend like a finger from the fatigue crack zone. Beyond the tip of the square zone the vein pattern typical of plane stress failure in these materials is evident [2, 3, 5, 13]. As catastrophic failure proceeds, shear deformation also occurs around the plane strain zone as evidenced by the smooth shear zone on its lower periphery. The low stress behaviour is similar in that a "finger", with attendant wide shear lips, extends from the fatigue crack but the final failure beyond this finger is still square with small shear lips. In either case it appears that catastrophic failure occurs only when the crack extends beyond the finger zone. Hence we expect that  $K_C$  should be estimated using the peak load and a crack length extending to the end of the narrow finger zone.

### 3.2. Fracture toughness

Fracture toughness values for the centre cracked tension configuration may be calculated using the formula given by Irwin *et al.* [14],

$$K_C = \sigma [W \tan(\pi a/W)]^{1/2} \quad (1)$$

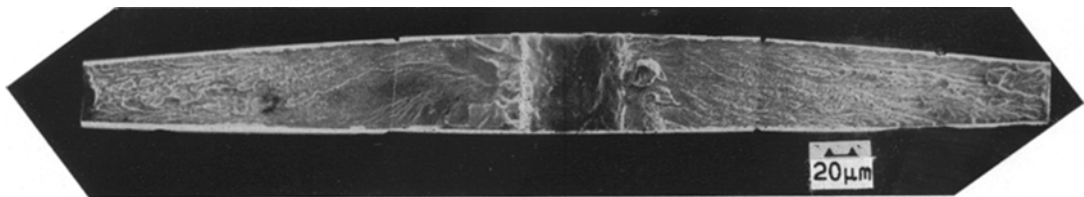


Figure 2 The continuous fracture surface of a  $\text{Ni}_{49}\text{Fe}_{29}\text{P}_{14}\text{B}_6\text{Si}_2$  metallic glass specimen (SEM). The EDM hole lies at the centre of the surface. The fatigue crack is contiguous to either side of the hole. The rapid fracture surface is at  $90^\circ$  to the specimen axis. No transition to slant behaviour is observed for these specimens.

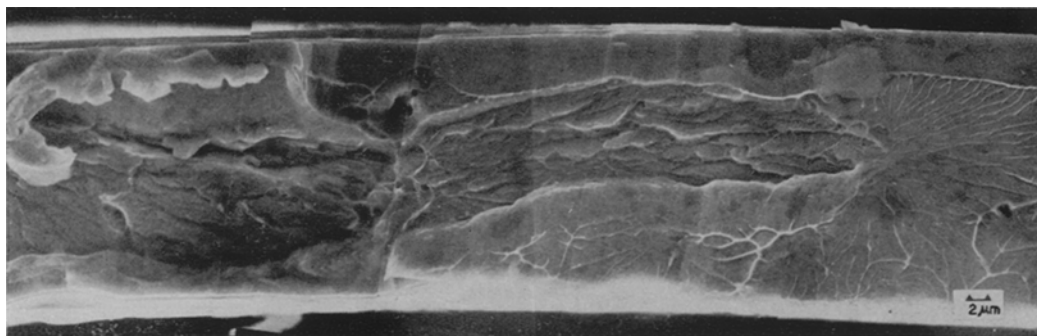


Figure 3 A portion of the fracture surface of a  $\text{Ni}_{48}\text{Fe}_{39}\text{P}_{14}\text{B}_6\text{Al}_3$  specimen exhibiting the transition from square to slant (right hand side) failure. The square zone has a "finger" shape.

where  $a$  is the crack half-length,  $W$  is the panel width and  $\sigma$  is the nominal stress. For the conditions of the present experiments this reduces to

$$K_C = \sigma \sqrt{(\pi a)}. \quad (2)$$

For the single edge notch geometry, Equation 2 may be used (with the total crack length equal to  $a$ ) with a multiplicative correction factor  $f[K_C = \sigma f \sqrt{(\pi a)}]$  to account for finite specimen dimensions [15].

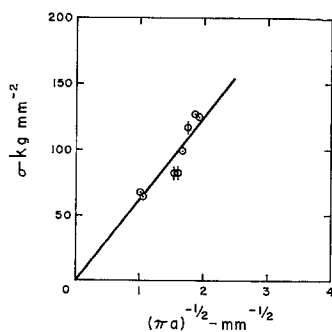


Figure 4 Nominal stress versus  $(\pi a)^{-1/2}$ , where  $a$  is the half-length of the fatigue crack, for  $\text{Ni}_{39}\text{Fe}_{38}\text{P}_{14}\text{B}_6\text{Al}_3$ . The slope of the line is  $K_C = 62 \text{ kg mm}^{-3/2}$ . The datum points marked with vertical slashes are those where the specimen was fractured at a constant stroke rate.

Fig. 4 presents the fracture toughness data for the  $\text{Ni}_{39}\text{Fe}_{38}\text{P}_{14}\text{B}_6\text{Al}_3$  alloy in the form of a plot of  $\sigma$  versus  $\sqrt{(\pi a)^{-1}}$ . For this alloy a reasonable variation in stable crack length was achieved and hence such a representation is meaningful. As expected, according to Equation 2, the data may be approximated by a straight line, the slope of

which is  $K_C = 62 \pm 5 \text{ kg mm}^{-3/2}$ , where the limits represent the average deviation from the mean value. Average  $K_C$  values of  $120 \pm 7$  (typically,  $\sigma \simeq 96 \text{ kg mm}^{-2}$ ,  $a \simeq 0.145 \text{ mm}$ ,  $f = 1.86$ ) and  $30.5 \pm 2 \text{ kg mm}^{-3/2}$  ( $\sigma \simeq 66.6 \text{ kg mm}^{-2}$ ,  $a \simeq 0.0667 \text{ mm}$ ) are observed for the  $\text{Ni}_{48}$  and  $\text{Ni}_{49}$  alloys, respectively. A value of  $56 \pm 6 \text{ kg mm}^{-3/2}$  is obtained for the  $\text{Ni}_{48}$  alloy if the extent of the fatigue crack is taken as the critical crack.

The  $K_C$  data for the Ni-Fe alloys are plotted in Fig. 5 as a function of specimen thickness. As prepared, the  $\text{Ni}_{39}$  and  $\text{Ni}_{49}$  (Fig. 2) strips are slightly thicker in the centre than at the edges. For the purposes of Fig. 5 the average thickness value at the sites of rapid fracture initiation (on opposite sides of the hole) is plotted for each specimen.

### 3.3. Fatigue crack propagation rate

A careful examination of the fatigue zones in Fig. 1a and b indicates the presence of surface striations. This is shown more clearly in Fig. 6 which is an enlarged view of part of the fatigue zone of Fig. 1a. Careful measurements of the striation spacing,  $S$ , were made and are plotted as a function of the cyclic stress intensity in Fig. 7. The line hand-drawn through the data suggests that  $S \simeq 1.2 \times 10^{-7} \Delta K^{2.25}$  where  $S$  has units of mm and  $\Delta K$  units of  $\text{kg mm}^{-3/2}$ . One may compare  $S$  with  $da/dn$ , the rate of fatigue crack advancement, determined by direct microscopic observations. For these experiments stress (load) times were set at  $\sigma_{\text{max}} = 63 \text{ kg mm}^{-2}$  and  $\sigma_{\text{min}} = 21 \text{ kg mm}^{-2}$ . Typical results are shown in Fig. 7. It appears that  $S$  and  $da/dn$  exhibit a parallel dependence on  $\Delta K$ ;  $S$ , however, exceeds

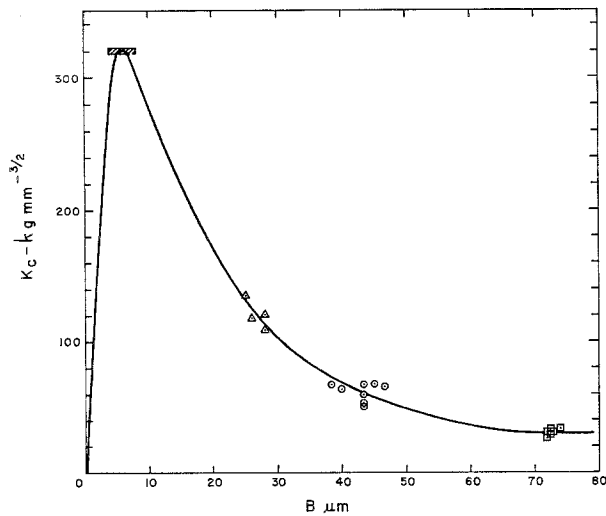


Figure 5 Fracture toughness,  $K_C$ , as a function of thickness for various metallic glasses. Triangles, circles and squares are for the  $Ni_{48}$ ,  $Ni_{39}$  and  $Ni_{49}$  alloys, respectively. The shaded bar represents data of Kimura and Masumoto [11] for  $Fe_{80}P_{13}C_7$  obtained from tear tests.

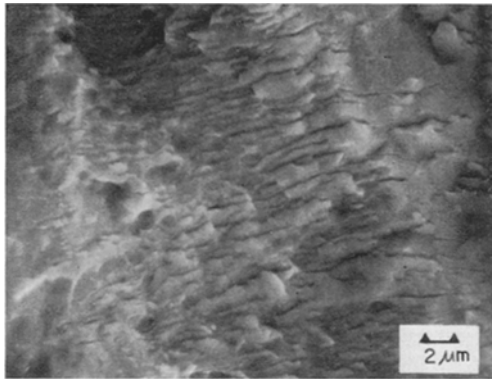


Figure 6 An enlarged portion of Fig. 1a showing striations on the fracture surface produced by fatigue. The direction of crack propagation is toward the bottom of the page.

$da/dn$  by a factor of  $\sim 6$  ( $da/dn \simeq 2 \times 10^{-8} \Delta K^{2.25}$ ).

4. Discussion

4.1. Fracture toughness

As discussed by Knott [10, p. 114] the fracture toughness,  $K_C$ , will increase as the mode of fracture changes from almost fully square (plane strain) to a mixed mode exhibiting increasingly greater amounts of slant (plane stress) fracture. This variation occurs with decreasing sample thickness as the ratio of plastic zone size to specimen thickness increases. Maximum toughness ( $K_{IIC}$ ) is reached at a thickness (approximately twice the single shear lip thickness in fully plane strain fracture) when the last vestiges of square fracture disappear.

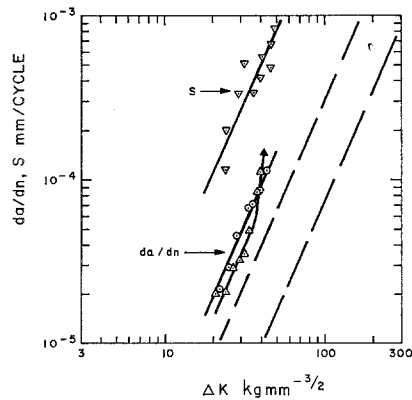


Figure 7 Fatigue crack propagation rate,  $da/dn$ , and striation spacing,  $S$ , as a function of  $\Delta K$ , the cyclic stress intensity for  $Ni_{39}Fe_{38}P_{14}B_6Al_3$ . The circles and triangles for  $da/dn$  are for two different specimens. For one ( $\Delta$ ) the crack appeared to exceed the  $\Delta K^{2.25}$  dependence near the end of life. The data for  $S$  ( $\nabla$ ) were obtained from several specimens. The dashed lines indicate the scatter band for structural steels. The upper bound curve is given by  $da/dn \simeq 9.8 \times 10^{-9} \Delta K^{2.25}$ .

With further decrease in thickness the fracture toughness again decreases because the ease of sliding off in mode III increases with decreasing thickness. Accordingly, one obtains a curve similar to that of Fig. 5, where we have plotted, at a thickness equal to twice the shear lip thickness for the Ni-Fe alloys ( $4$  to  $8 \times 10^{-3}$  mm), the  $K_{IIC}$  ( $= 320 \text{ kg mm}^{-3/2}$ ) value obtained by Kimura and Masumoto [11] for amorphous  $Fe_{80}P_{13}C_7$ . Given that the Ni-Fe alloys examined here have the same structure (amorphous) and that the inherent yield strength

of all three alloys is of the order of  $250 \text{ kg mm}^{-2}$ , it would appear that compositional differences alone should not result in significant variation of their fracture toughness properties. We conclude, therefore, that the variation in  $K_{IC}$  for the Ni-Fe alloys is primarily a thickness effect, as suggested by Fig. 5.

As also discussed by Knott, a minimum fracture toughness  $K_{IC}$ , constant with further increase in thickness, obtains when fully plane strain failure is achieved. A question of some interest is whether the thickest specimen tested here ( $\text{Ni}_{49}$ ) exhibits a true  $K_{IC}$  value. Although no transition to slant behaviour occurs as the crack runs it is conceivable that square fracture can occur without maximum plane strain constraint throughout the specimen. The conditions cited [10] for determination of a valid  $K_{IC}$  include: (1)  $W - a \geq a \geq B$ , where  $B$  is the specimen thickness, (2)  $r_{IY} \leq 0.02a$ , where  $r_{IY}$  is the radius of the plane strain plastic zone, and (3)  $B \geq 2.5 (K_{IC}/\sigma_y)^2$ , where  $\sigma_y$  is the yield stress. For the  $\text{Ni}_{49}$  alloy, condition (1) was met as  $B$  (0.07 mm) is approximately equal to  $a$  ( $\sim 0.06$  mm) and both are much less than  $W - a$  ( $\sim 0.7$  mm). Conditions (2) and (3) may be considered in terms of the radius of plane stress plastic zone

$$r_y = (K_{IC}/\sigma_y)^2/2\pi. \quad (3)$$

We have then  $r_{IY} \simeq r_y/3$  and  $B \simeq 15r_y$ . Assuming  $r_y \simeq t_0$ , the shear lip thickness, yields  $r_y \simeq 3 \times 10^{-3}$  mm; then  $r_{IY} \simeq 10^{-3}$  mm so that  $a_{\min} \simeq 0.05$  mm and  $B \geq 0.045$  mm. Hence conditions (2) and (3) are met for the  $\text{Ni}_{49}$  alloy. Using Equation 3 with  $r_y = 3 \times 10^{-3}$  mm and  $\sigma_y \simeq 250 \text{ kg mm}^{-2}$  one may also calculate  $K_{IC} \simeq 34 \text{ kg mm}^{-3/2}$ . This is close to the value observed. We conclude that  $K_{IC}$  for amorphous Ni-Fe base alloys is  $\simeq 30 \text{ kg mm}^{-3/2}$ .

A comparison of this value with representative toughness values for crystalline ferrous alloys is of interest but somewhat difficult. Data are available for steels with yield strengths ranging up to  $\sim 200 \text{ kg mm}^{-2}$ , in which case values as high as  $250 \text{ kg mm}^{-3/2}$  are quoted for 18% Ni maraging steel [16]. Toughness values for quenched martensitic steels at this stress level fall in the range of  $170 \text{ kg mm}^{-3/2}$  [16]. In all cases, however, the data indicate a sharp decrease of  $K_{IC}$  with increasing  $\sigma_y$ , so that, for a steel with an inherent yield stress of  $\sim 250 \text{ kg mm}^{-2}$ , a toughness value ( $K_{IC}$ ) of the order of  $50 \text{ kg mm}^{-3/2}$  may obtain. Such a value is comparable to that reported here for Ni-Fe metallic glasses.

It must also be considered that Young's modulus ( $E$ ) for the Ni-Fe metallic glasses is significantly less than for steel. Using the shear modulus data of Pampillo and Polk [5] for  $\text{Ni}_{49}\text{Fe}_{29}\text{P}_{14}\text{B}_6\text{Al}_2$  and assuming a Poisson ratio of 0.3 one obtains  $E \simeq 1.53 \times 10^4 \text{ kg mm}^{-2}$  ( $21.7 \times 10^6$  psi). The same value was measured directly by Berry and Prichet [17] for  $\text{Fe}_{75}\text{P}_{15}\text{C}_{10}$ . Hence to make a meaningful comparison with steel, the  $K_{IC}$  value observed for Ni-Fe metallic glasses should be normalized with a factor of  $\sim 3/2$ .

## 4.2. Fracture topography

Examination of the plane strain fracture region (chevron pattern), indicates that it is perpendicular to the tensile axis only on a gross scale. In detail it consists of a sawtooth pattern with surfaces inclined to the tensile axis. Examination of opposing fracture surfaces indicates that a "valley" on one surface is matched by a "peak" on the other surface. Closer inspection, as in Fig. 8a and b, reveals that the chevron surfaces are marked by a fine scale, equiaxed vein pattern. It seems likely, therefore, that these surfaces are produced by shear rupture. One expects that the scale of the vein pattern (compare Figs. 3 and 8) may vary inversely as the local yield stress. Under the plane strain constraint (Fig. 8) the local yield stress would be raised to  $\sim 3$  times its normal value.

The striations observed on the fatigue fracture surface show, on the other hand, no evidence of a vein pattern. It appears that the fatigue crack is produced under pure alternating shear conditions.

## 4.3. Fatigue crack propagation rate

Fig. 7 shows for comparison two dashed lines representing the fatigue crack propagation rate scatter band in crystalline ferrous alloys as given by Clark [18]. It is evident that, for given  $\Delta K$ , the propagation rate is slightly higher in the  $\text{Ni}_{39}$  amorphous alloy. This difference is removed, however, if one plots the respective data as functions of  $(\Delta K/E)$ , as in Fig. 9, where the upper bound solid line for steel is given by  $da/dn \simeq 52.5 (\Delta K/E)^{2.25}$ . Such a comparison suggests that the crack propagation rate may be dependent on the relative magnitudes of crack tip opening displacement,  $\delta$ , and the plastic zone size. That is  $\delta \simeq K_I^2/2E\sigma_y$  [19]. Using Equation 3 this may be rearranged to give  $\delta \simeq \frac{1}{2} (2\pi r_y)^{1/2} (K_I/E)$ , so that  $\delta/\sqrt{r_y} = (\sqrt{(2\pi)/2}) (K_I/E)$ .

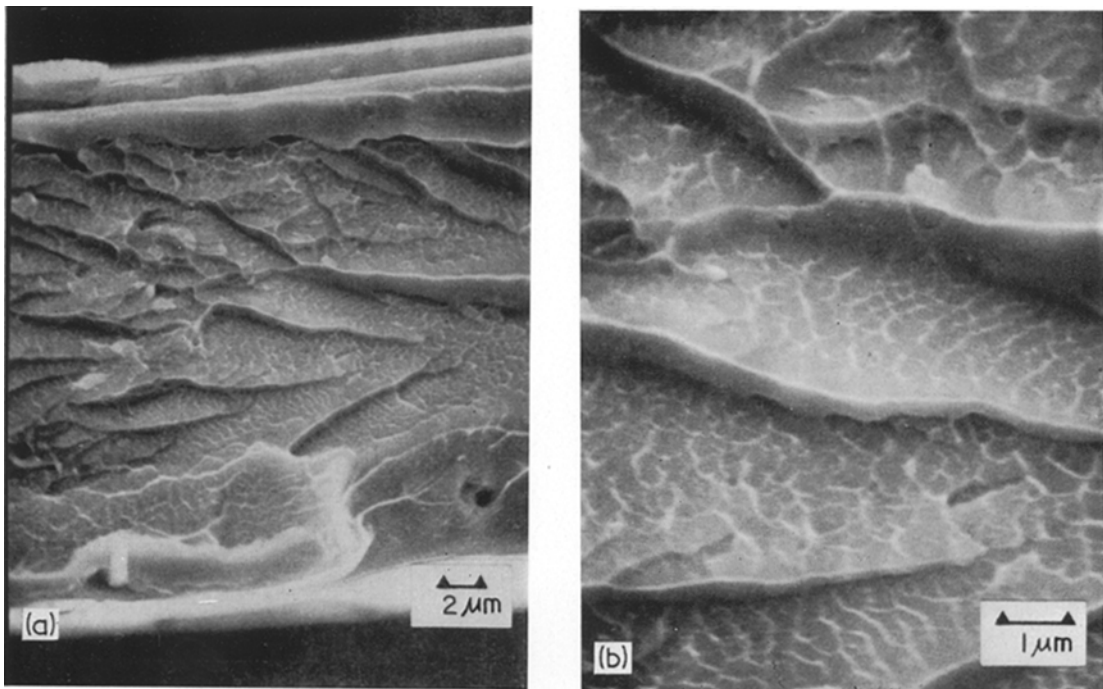


Figure 8 (a) A view of the chevron pattern surface for a  $\text{Ni}_{48}$  specimen. (b) An enlarged view of 8 (a). A fine scale, equi-axed vein pattern is evident on the chevron surfaces. The crack propagation direction is to the left in each case.

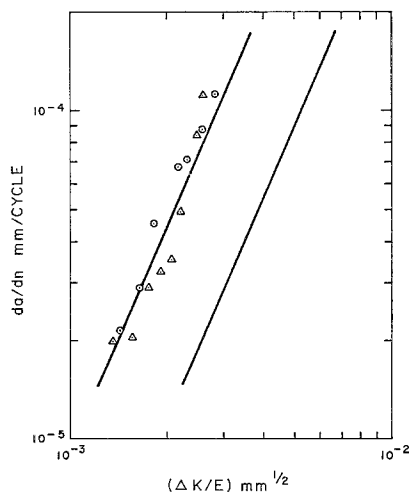


Figure 9 Fatigue crack propagation rate as a function of  $(\Delta K/E)$  for the  $\text{Ni}_{39}$  alloy. The solid lines are the scatter band found for crystalline ferrous alloys (see text).

At the level of inspection provided by the scanning electron microscope one cannot observe striations (if, indeed, they exist) corresponding to the fatigue crack advancement for each cycle of stress,  $da/dn$ . The spacing,  $S$ , observed (Figs. 1

and 6) is about 6 times larger than  $da/dn$  (Fig. 7). One expects that the observed striations occur because the local direction of crack propagation is always inclined (at  $\pm 45^\circ$  in the Bilbey-Swinden model [20]) to the crack plane. The oscillation in local direction should occur with a period (striation spacing) comparable to the plastic zone size. Using Equation 3 with  $\Delta K = 30 \text{ kg mm}^{-3/2}$  we may calculate that the cyclic plastic zone size  $\Delta r_{IY} = \Delta r_y/3 \simeq 8.3 \times 10^{-4} \text{ mm}$ ; the corresponding value of  $S$ ,  $2 \times 10^{-4} \text{ mm}$ , is of comparable magnitude.

## 5. Conclusions

When tested in tension, unnotched strips of metallic glasses, including the Ni-Fe glasses examined here, fail in the shear mode (plane stress). Their fracture surfaces exhibit a featureless shear deformation zone and a zone marked by a vein pattern, produced by shear rupture. When tensile failure occurs in the presence of a sharp, fatigue induced crack, the same strips exhibit varying degrees of square (plane strain) fracture, depending on sample thickness. The plane strain zone, macroscopically at  $90^\circ$  to the tensile axis, is marked by a classical chevron

pattern. However, the chevron surfaces are marked by a fine scale, equi-axed vein pattern, indicating that local failure occurs by shear rupture.

The fracture toughnesses of the  $\text{Ni}_{48}\text{Fe}_{29}\text{P}_{14}\text{B}_6\text{Al}_3$ ,  $\text{Ni}_{39}\text{Fe}_{38}\text{P}_{14}\text{B}_6\text{Al}_3$  and  $\text{Ni}_{49}\text{Fe}_{29}\text{P}_{14}\text{B}_6\text{Si}_2$  metallic glasses are observed to be  $120 \pm 7$ ,  $62 \pm 5$  and  $30 \pm 2$   $\text{kg mm}^{-3/2}$ , respectively. These values apparently decrease in the order of increasing plane strain constraint, i.e., increasing thickness. The value observed for the  $\text{Ni}_{49}$  glass appears to be a valid plane strain fracture toughness, characteristic of the Ni-Fe base amorphous alloys, i.e.,  $K_{IC} \approx 30$   $\text{kg mm}^{-3/2}$ .

Fatigue crack propagation occurs in the  $\text{Ni}_{39}$  metallic glass at a rate given by  $da/dn \approx 2 \times 10^{-8} \Delta K^{2.25}$ , where units of kg and mm are used. This rate lies slightly above the scatter band observed for crystalline ferrous alloys for the same  $\Delta K$ . One may account for this difference if both sets of data are plotted in terms of  $(\Delta K/E)$ .

### Acknowledgements

Thanks are due to Dr Donald Polk, Mr John Bedell and Mr Naim Hemmat, each of whom provided strips of one of the alloys tested. The author is again indebted to Mrs Annemarie Reimschuessel for co-operation in use of the scanning microscope, to Miss Patricia Brady for assistance with the microscopy and Mr Richard Fehrman for assistance with the mechanical testing.

### References

1. T. MASUMOTO and R. MADDIN, *Acta Met.* **19** (1971) 725.
2. H. J. LEAMY, H. S. CHEN and T. T. WANG, *Met. Trans.* **3** (1972) 699.
3. L. A. DAVIS and S. KAVESH, *J. Mater. Sci.* **10** (1975) 453.
4. D. E. POLK and C. A. PAMPILLO, *Scripta Met.* **7** (1973) 1161.
5. C. A. PAMPILLO and D. E. POLK, *Acta Met.* **22** (1974) 741.
6. H. S. CHEN, H. J. LEAMY and M. J. O'BRIEN, *Scripta Met.* **7** (1973) 415.
7. C. A. PAMPILLO and H. S. CHEN, *Mat. Sci. Eng.* **13** (1973) 181.
8. H. S. CHEN, *Scripta Met.* **7** (1973) 931.
9. A. S. TETELMAN and A. J. MCEVILY, JUN, "Fracture of Structural Materials" (John Wiley, New York, 1967) p. 38.
10. J. F. KNOTT, "Fundamentals of Fracture Mechanics" (Butterworths, London, 1973).
11. H. KUMURA and T. MASUMOTO, *Scripta Met.* **9** (1975) 211.
12. A. H. COTTRELL, "The Mechanical Properties of Matter" (John Wiley, New York, 1964) p. 342.
13. C. A. PAMPILLO and A. C. REIMSCHUESSEL, *J. Mater. Sci.* **9** (1974) 718.
14. G. R. IRWIN, J. A. KIES and H. L. SMITH, *Proc. Amer. Soc. Test. Mat.* **58** (1958) 640.
15. C. C. OSGOOD, *Machine Design*, August 19 (1971) 102.
16. V. F. ZACKAY, E. R. PARKER, J. W. MORRIS, JUN and G. THOMAS, *Mat. Sci. Eng.* **16** (1974) 201.
17. B. S. BERRY and W. C. PRITCHETT, *J. Appl. Phys.* **44** (1973) 201.
18. W. G. CLARK, JUN, *ASM Metals Eng. Q.* August (1974) 16.
19. G. T. HAHN, M. F. KANNINEN and A. R. ROSENFELD, *Ann. Rev. Mat. Sci.* **2** (1972) 381.
20. B. A. BILBY and K. H. SWINDEN, *Proc. Roy. Soc. Lond.* **A285** (1965) 22.

Received 31 December 1974 and accepted 23 January 1975.